To Journal of Earthquake and Tsunami

Mesoscale Modeling of Concrete under Dynamic Split Tension

Xiao-Qing Zhou
Associate Professor,
College of Civil Engineering, Shenzhen University,
Shenzhen, Guangdong, China
E-mail: xqzhou@szu.edu.cn

Yong Xia
Associate Professor,
Department of Civil and Environmental Engineering, The Hong Kong Polytechnic University,
Hong Kong, China
E-mail: ceyxia@polyu.edu.hk

Abstract

In the present paper, a mesoscale model is adopted to model the concrete behavior under dynamic split tension. The concrete material is assumed to consist of coarse aggregates, mortar matrix, and interfacial transition zone (ITZ). In the mesh generation process, random coarse aggregate particles are generated from a certain aggregate size distribution and then placed into the mortar matrix with ITZ between the coarse aggregate edge and the mortar matrix. Different aggregate shapes, i.e., circular, oval, and polygons, are modeled to analyze the gravel and crushed stone aggregates, respectively. Numerical simulation is used to model the dynamic damage responses of a typical cylinder specimen and a typical cube concrete specimen under split tension. Velocity boundary is added as a dynamic loading. Computational results obtained agree well with the normal experimental results. On the macroscale level, reasonable tensile stress-strain relationships are calculated; on the mesoscale level, the detailed stress wave distribution and the crack pattern are obtained, it can be found that the cracks are affected by the aggregate distribution.

Keywords: Mesoscale model, concrete, split tension, interfacial transition zone (ITZ)

1. Introduction

As a common construction material, concrete is widely used to construct bridges, civil structures, nuclear plants and military facilities all over the world. Those structures might be subjected to impact or explosive loading during their service life. Terrorist attack and accidental explosion are two typical highly dynamic loading cases. It is of interest for researchers to study the static and dynamic behaviours of concrete. Under dynamic loading, the behaviour of concrete-like material is well known to be strain rate dependent (Malvar and Ross, 1998, Grote et al. 2001, Song and Lu, 2012). Typically SHPB (Split Hopkinson Pressure Bar) apparatus can be used to test the compressive dynamic mechanism of concrete under different loading rates (Gomez et al., 2001, Zhang et al., 2009). To perform tensile splitting experiments under dynamic loading, SHPB can also be used to test the dynamic tensile strength of concrete (Gomez et al., 2001). Numerical simulation has also been employed to analyze the behaviour of concrete sample under this kind of dynamic tensile loading (Hughes et al., 1993, Zhu and Tang, 2006).

In numerical simulations, concrete can be simulated in different scales, say, macroscopic, mesoscopic, and microscopic scales. In the macroscopic scale modelling, the concrete material is normally assumed to be isotropic and homogeneous. Many constitutive relationships have been constructed to model the behaviour of concrete. For example, the RHT model (Riedel et al. 1999) used in AUTODYN (AUTODYN

2005), Gebbeken model (Gebbeken 2000), and K&C model (Malvar et al., 1997) used in LS-DYNA (2007). Concrete is a typical composite material consisting of coarse aggregates, fine aggregates and cement pastes, with some additives if necessary. The concrete mesoscale structure makes its behaviour rather complicated. Especially, high strain rate loading cases often generates stress waves traveling inside the concrete member. Consequently the distribution of the stress field inside the concrete is highly non-homogeneous. Therefore, the use of a mesoscale concrete model is desirable to capture the concrete material response when it is under high strain rate. To analyse the detailed concrete damage responses under different loading cases, mesoscale models have been constructed (Wang et al., 1999, Wriggers and Moftah 2006, Zhou et al., 2009, Unger and Eckardt, 2011). In a mesoscale concrete model, coarse aggregates, mortar matrix and the interfacial transition zone (ITZ) are often modelled by different material constitutive models. Most of the mesoscale simulations of concrete are focused on the static response of concrete-like materials. Some studies have been done to apply the mesoscale models in dynamic numerical simulations to investigate the dynamic material properties of concrete (Zhou and Hao, 2008, Lu et al., 2009, Song and Lu, 2012). In our previous work (Zhou and Hao, 2008), mesoscale modelling has been done to investigate the dynamic responses of a typical cylinder splitting test, where simplified circular aggregates were the only shape considered. Professor Lu and his co-workers have done some mesoscale numerical researches on the high strain rate compressive behaviours (Lu et al., 2009, Song and Lu, 2012), where polygonal shapes are adopted to model the coarse aggregates. Xu et al. (2012) have analysed the

dynamic tensile behaviour of fibre reinforced concrete. At microlevel, the mortar matrix of the mesoscale level is subdivided into fine aggregate and hardened cement paste. Very high computational cost makes the microscopic simulation unaffordable. Therefore, mesoscale simulation is adopted in the present study.

In the present paper, the typical split tension tests of a cylinder concrete specimen and a cube concrete are numerically simulated by a mesoscale concrete model. In the mesoscale model, the coarse aggregates are modeled by different shapes, say, circular, oval and polygons. Numerical simulation results of different cases are obtained, especially the effect of the coarse aggregate shape is analyzed.

2. Mesoscale Model

At the mesoscale level, concrete can be regarded as being composed of three different phases, coarse aggregates, mortar matrix and ITZ. Figure 1 shows a typical section view of a concrete sample (Zhou et al, 2009). It was scanned by CT. From the figure, coarse aggregates and mortar matrix can be clearly seen. In the present study, the coarse aggregates, mortar and the ITZ are distinctively simulated with the respective material properties.

2.1. Mesoscale Concrete Structure

The mesoscale concrete structure to be generated consists of randomly distributed coarse aggregate particles and the mortar matrix filling the space between the particles. Therefore, the layout of the mortar matrix depends entirely on the spatial distribution of the aggregate particles.

The generation of the random coarse particles must satisfy the basic statistical characteristics of the real concrete material. In addition, the spatial distribution of the aggregate particles must be as macroscopically homogeneous in space and macroscopically isotropic as possible (Wriggers and Mofta, 2006).

The popular “take-and-place” method is adopted here to generate the coarse aggregates. The random principle is applied by taking samples of aggregate particles and placing the aggregate particles one by one into the concrete in such a way that there is no overlapping with particles already placed. The size distribution of the particles must follow a certain given grading curve.

2.2. Generation of Coarse Aggregates

For normal concrete, coarse aggregates refer to the particles whose diameters are greater than 4.75 mm. For most concrete, the coarse aggregates represent 40–50% of the concrete volume. The shape of the coarse aggregate particles depends on the aggregate type. In general, gravel aggregates have a rounded shape while crushed stone

aggregates have an angular shape. In the present study, circular and oval particles are adopted to model gravel aggregates, while the polygons are used to model the rushed stone aggregates.

2.2.1 Aggregate Size Distribution

The determination of the particle size distribution for aggregates is usually expressed in terms of the cumulative percentage passing through a series of sizes of sieve openings. One of the most acceptable aggregate distributions is given by Fuller (Wriggers and Mofta, 2006) as:

$$P(d) = 100\left(\frac{d}{d_{\max}}\right)^{n} \tag{1}$$

where $P(d)$ is the cumulative percentage passing a sieve with an aperture diameter of d, d_{max} is the maximum size of the aggregate particles, and n is the exponent (n = 0.45–0.70). In the practical concrete construction, the typical maximum size of aggregates is about 32 mm to obtain high quality concrete mix. Fuller's grading curve is shown in Figure 2, where d_{max} is assumed to be 32 mm and n is taken as 0.5. In the present study, since the concrete-like specimens considered have much smaller sizes compared with normal concrete member, the maximum coarse aggregate size, d_{max}, is set as a smaller size, 10mm. In addition to that, the minimum aggregate size is assumed to be 2.5mm, which is smaller than the most frequently used number of 4.75mm.

In the numerical simulation, the grading curve expressed in Eq.1 can be discretized into a certain number of segments (Lu and Tu, 2009), each covering a size range of [d_i,

d_{i+1}]. Thus the amount (area in 2D) of aggregates within each grading segment is

$$A_{a,i} = \frac{P(d_{i+1}) - P(d_i)}{P(d_{\max}) - P(d_{\min})} \times A_a \tag{2}$$

where A_a is the total amount (area in 2D) of aggregates in concrete and d_{min} is taken as 2.5 mm in the present study.

2.2.2 Aggregate Particle shapes

The circular, oval, and polygonal shaped aggregate particles are respectively constructed in the present study. The circular shape aggregates can be easily constructed. Uniformly distributed random numbers are set to determine the centers of the circles. The diameters are then generated randomly. As for the oval shaped aggregates, random numbers are generated to determine the position of the oval center *(x,y)*, long axial radius r_l, short axial radius r_s , and the orientation angle of the long axis φ. Typical oval particle with those randomly distributed parameters is shown in Figure 3. For simplicity, the polygon aggregates are constructed as the inscribed polygons of the ovals, with the side number randomly distributed between 6 and 12 and the interior angles randomly distributed between 15 and 90 degrees, avoiding weird shapes. Figure 4 shows a typical polygonal shaped aggregate. As for those polygonal particles in the circular specimen, only random quadrangular shapes are adopted.

2.2.3 Aggregates Placing Process

The typical circular particles placing process is as follows,

Step 1. Calculate the area of aggregates to be generated in the grading segment.

Step 2. Generate a uniformly distributed random number to determine the position of the aggregate particle (center of the circle).

Step 3. Generate a random number defining the size of an aggregate particle, assuming the particle size d is a uniformly random number between size range of [d_i, d_{i+1}]. Largest size range is put first.

Step 4. Check whether all the placing conditions are completely satisfied. The placing conditions include: overlap between any two particles, or overlap between a particle and any edge is not allowed; a minimum gap size t needs to be provided between any two particles. As shown in Figure 5, those dashed circles are unsuccessful and should be avoided.

Step 5. Calculate the total area of the generated aggregate particles and compared with the area within the current grading segment. If the former is less than the latter, repeat from Step 2; otherwise, calculate the next grading segment.

Step 6. Repeat the above steps for the next grading segment until the total area of aggregates reaches a certain value, which means that all the particles are generated.

For oval and polygonal shaped particles, the placing process is similar to that for the circular particles. The differences are the process in avoiding overlap and area calculation, which are more difficult for oval and polygonal particles.

Typical aggregate particles for different shapes are shown in Figure 6. ITZ is clearly

shown in the figure as a thin boundary around the aggregates.

2.3 Material Models for three phases

Hydrocode is adopted in the present study (AUTODYN 2005). The equation of state (EOS) and the strength criterion need to be constructed to model the three phases in concrete. A piecewise-linear porous model (Zhou and Hao, 2009) is used to model both the mortar matrix and the ITZ. The simplest linear EOS is adopted to model the aggregate as follows,

$$p = k\mu \tag{3}$$

where p is the pressure, $\mu=(\rho/\rho_0)-1$, and k is the material bulk modulus. Obviously the modulus of aggregate is much higher than that of the mortar matrix.

The deviatoric stress tensor is governed by a damage-based yield strength surface. The dynamic yield strength surface is amplified from the static surface by considering the strain rate effect. Typically the compressive (tensile) strength is multiplied by a compressive (tensile) dynamic increase factor (DIF). Due to the lack of the experimental results, determination of the DIFs for ITZ is assumed to be the same as that for the mortar matrix. The yield strength criterion considered is a piece-wise Drucker-Prager model. The equivalent yield strength can be determined by

$$F_p = \sqrt{J_2} - b_i p - a_{id} \le 0 (i = 1 \sim N) \tag{4}$$

where J_2 is the second invariant of the stress deviatoric tensor, p is the hydrostatic

pressure, and other parameters are used to determined piece-wise linear model.

For the coarse aggregate and mortar matrix, same material constants as those in our previous work (Zhou and Hao, 2009) are adopted here. As for the ITZ, the material constants for the strength and Young's modulus are assumed as 75% of the mortar matrix. The material parameters for all the three phases are listed in Table 1.

3. Numerical Simulation

3.1 Split Tension Test Setup and Numerical Model

In order to analyze the dynamic behaviour of concrete material under different strain rates, two-dimensional models of concrete mixture are constructed and modelled. Two split tension specimens are modelled in the present study, one is the typical cylinder specimen (the same specimen as that in our previous work, Zhou and Hao, 2008), and the other is a cube concrete sample. Numerical model and boundary condition for the cylinder case are shown in Figure 7. The diameter of the specimen is assumed to be 50mm, In this figure, it can be seen that the vertical velocity is added as a boundary condition on the upper side of the circle, while the displacement is fixed on the lower bound of the circle. In the present study, only one typical constant velocity, 1m/s, is considered. Three different coarse aggregate shapes adopted in the present simulation are shown in Figure 8.

In China, a cube concrete sample with a length of 150 mm is the typical specimen for the split tension test. A typical split tension test setup of the cube specimen is shown in Figure 9. The model geometry in the numerical simulation is shown in Figure 10. The bottom boundary shown in the figure is assumed to be fixed, while velocity boundary shown in Figure 11 is added on the top boundary. The element size is chosen as 0.5 mm, resulting in a total element number of 300×300.

3.2 Numerical Results

3.2.1 Numerical Results of the cylinder Specimen

In numerical simulation of the cylinder specimen, four different cases are studies, i.e. (a) homogeneous model, (b) mesocale model with random circular aggregates, (c) random oval aggregate mesoscale model and (d) random polygon mesoscale model. For these mesoscale models, their aggregate distributions are shown in Figure 8. Fig.12 shows the σ_{xx} distribution at different time instants. For comparison, homogeneous model, mesoscale models with different aggregate shapes are shown in the figure. From the figure, the stress wave propagation can be clearly seen. The effect of the aggregate and the ITZ is also noticeable. For the cases from (b) to (d), their stress distributions are obviously not as continuous as that in case (a). Especially, the stress state in the ITZ elements differs a lot from their neighbor elements. The reason is that different material properties of the three phases inside the concrete specimen affect the

stress wave transportation. From detailed comparison it can be found that sometimes the ITZ elements are in compression when their neighbor elements are in tension.

For all the three cases, the first failure occurs in the ITZ somewhere along the middle line, then the major crack generates. The failure modes for the above four cases are shown in Figure 13. In this figure, it can be clearly seen that the crack pattern is affected by the aggregate distribution. Basically, the maximum tensile stress occurs along the middle line, thus the cracks occur along this line. However, the position of the aggregate does affect the crack pattern because the cracks only occurs along the ITZ and the mortar matrix element, while the aggregate is still kept intact. For the mesoscale cases of (b), (c) and (d), the crack pattern in case (d) shows failure pattern which is more realistic to the real experimental tests, where an obvious main crack along the center line can be found; while for the other two cases, more cracks in the ITZ areas around the center line can be found. From this point of view, polygonal aggregate shape seems more reasonable, this is true because more crushed stone aggregates are used in the real concrete material.

Dynamic tensile strength is approximately obtained here by taking the average maximum stress over the middle 60% length of the central line. For all the mesoscale cases, the calculated dynamic strengths are around 5MPa, which is higher than the static tensile strengths of the mortar and the ITZ. This is caused by the strain rate effect because the dynamic increase factors (DIF) are considered for both the mortar matrix

and the IZT.

3.2.2 Numerical Results of the cube Specimen

For the polygonal aggregate model, the stress distribution (σ_{xx}) at different time instants is shown in Figure 14. With the increase of the time step, the stress becomes higher. Because the material properties for the three phases are not the same, the aggregate distribution affects the stress distribution. In particular, the stress in the ITZ differs a lot from that in the aggregate. This observation is the same as that in the cylinder specimen in the previous section. At the time of 0.1 ms, initial cracks can be clearly seen at around the centre of the specimen. The crack firstly occurs at the ITZ element. Accordingly, the stress in the ITZ element drops as the cracks begin to occur.

From the numerical simulation, it can be found that the total stress can still increase even the first few cracks occur because the rest part of the specimen can still support the loading. When more cracks happen, the stress drops gradually. The final crack pattern is shown in Figure 15. It shows that main vertical cracks occur along the centerline. Basically the specimen will be split into two halves, same as usual split tension tests.

The tensile stress-train relationship calculated from the mesoscale concrete with polygonal aggregate particles is shown in Figure 16. The tensile strength is around 3 MPa, which is slightly higher than the tensile strength of ITZ, but lower than that of

the mortar matrix. It is worthy noting that the dynamic loading obtained from the cube specimen is lower that from the cylinder specimen, because the strain rate in the cylinder specimen is higher since the size of the specimen is smaller. Another reason is that the thickness of ITZ in the cylinder specimen is 0.2mm, which in much smaller than that in the cube specimen, 0.5mm.

For the oval and circular aggregate cases, the numerical stress-strain relationship results obtained are similar as that shown in Figure 14. However, the stress distribution and the crack pattern are different from those shown in Figures 12 and 13. The reason is that the stress distribution and the crack pattern are affected by the aggregate position. Nevertheless, the overall responses of the entire specimen for different cases are similar.

5. Conclusions

A mesoscale concrete material is constructed in the present paper. Different shapes are used to mode the coarse aggregate particles. For the three phases in the concrete mixture, say, coarse aggregates, mortar matrix and ITZ, are modelled by different material models and different material parameters. The typical split tension test of a cylinder concrete specimen and a cube concrete specimen are modelled in two-dimensional mesoscale models. Numerical results show that reasonable entire stress-strain relationship can be obtained by the current mesoscale model. It can also be

found that the crack pattern and the stress distribution are affected by the aggregate shape, size and distribution. With the increase of the loading, the tensile stress increases. At the certain time instance, the first crack occurs at the ITZ element and then spreads through the mortar matrix. For the current loading case, cracks are not found in the aggregate particles.

The present numerical study shows that the mesoscale concrete model can obtain not only the mesoscale damage process, but also the macroscale stress-strain relationship.

ACKNOWLEDGEMENTS

The work performed in this paper is supported by the National Natural Science Foundation of China (Project No. 51078235).

REFERENCES

Autodyn, Century dynamics(2005), theory manual, Concord, California, USA. Century dynamics.

Gebbeken N, Ruppert M. A new material model for concrete in highdynamic hydrocode simulations. Arch Appl Mech 2000;70, 463–78.

Gomez JT, Shukla A, Sharma A (2001). Static and dynamic behaviour of concrete and granite intension with damage. Theoretical and Applied Fracture Mechanics. 36, 37-49.

Grote DL, Park SW, Zhou M (2001). Dynamic behaviour of concrete at high strain rates and pressure: I. experimental characterization, International Journal of Impact Engineering, 25,869-886.

Häfner S., Eckardt S., Luther T., Könke C. (2006), Mesoscale modelling of concrete: Geometry and numerics. Computers and Structures, 84, 450–61.

Hughes ML, Tedesco W, Ross CA. (1993), Numerical analysis of high strain rate splitting-tensile tests. Computers and Structures. 47,653-671.

Lin, Z, Wood, L. (2003), Concrete uniaxial tensile strength and cylinder splitting test. Journal of Structural Engineering. Vol.129, p. 692-698.

LS-DYNA (2007), Keyword User's Manual, Version 971, Livermore Software Technology Corporation.

Lu, Y., Song, Z.H., Tu, Z.G.(2009), Mesoscale analysis of concrete material under dynamic loading. International Workshop on Structures Response to Impact and Blast. 15-17 November 2009, Haifa, Israel. Paper 6-3.

Malvar, L.J., Crawford, J.E. and Wesevich, J.W. (1997), A plasticity concrete material model for Dyna3D , International Journal of Impact Engineering., 9-10(19), 847-873.

Malvar LJ, Ross CA(1998). Review of strain rate effects for concrete in tension, ACI Materials Journal, 95, 735-739.

Riedel W, Thoma K, Hiermaier S, Schmolinske E. (1999), Penetrating of reinforced concrete by BETA-B-500 numerical analysis using a new macroscopic concrete model for hydrocodes. In: Proceedings of ninth international symposium of IEMS, Berlin, p. 315–22.

Song, Z, and Lu Y (2012), Mesoscopic analysis of concrete under excessively high strain rate compression and implications on interpretation of test data. International Journal of Impact Engineering., 46,41-55.

Unger, J.F., Eckardt, S. (2011), Multiscale Modeling of Concrete: From Mesoscale to Macroscale. Archives of Computational Methods in Engineering, 18, 341–393.

Wang, Z.M., Kwan, A.K.H., and Chan, H.C. (1999), Mesoscopic study of concrete I: generation ofrandom aggregate structure and finite element mesh. Computers and structures, 70, 533-544.

Wriggers, P., and Moftah S. O. (2006). Mesoscale models for concrete: homogenisation and damage behaviour. Finite Elements in Analysis and Design, 42, 623–636.

Xu, Z., Hao, H. and Li, H.N. (2012). Mesoscale modelling of dynamic tensile behaviour of fibre reinforced concrete with spiral fibres. Cement and Concrete Research, 42,1475-1493.

Zhang M., Wu HJ, Li QM, Huang FL. (2009), Further investigation on the dynamic compressive strength enhancement of concrete-like materials based on split Hopkinson pressure bar tests, Part I: experiments. International Journal of Impact Engineering, 36, 1327-1334.

Zhou, S., Dang, F. , Chen, H., Liu, Y. (2009), Fracturing analysis of concrete meso structure under the uniaxial compression test with CT scan, The Ocean Engineering, 29:2, 89-95. (in Chinese).

Zhou, X.Q. and Hao, H. (2008). Mesoscale modelling of concrete tensile failure mechanism at high strain rates, Computers and Structures, 86, 2013-2026.

Zhou, X.Q. and Hao, H. (2009). Mesoscale modelling and analysis of damage and fragmentation of concrete slab under contact detonation, International Journal of Impact Engineering, 36,1315-1326.

Zhu WC, Tang CA. (2006), Numerical simulation of Brazilian disk rock failure under static and dynamic loading. International Journal of Rock Mechanics & Mining Sciences. 43, 236-252.

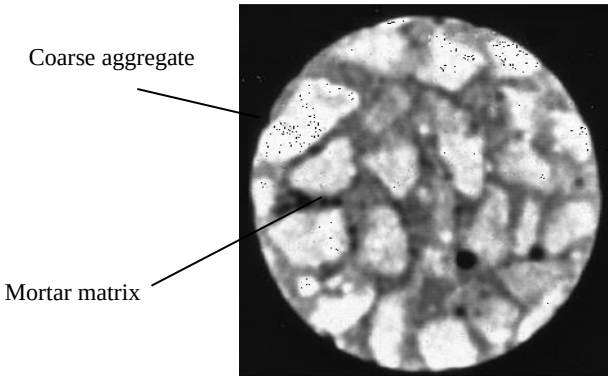

Figure 1. Typical section view of concrete sample (Zhou et al, 2009)

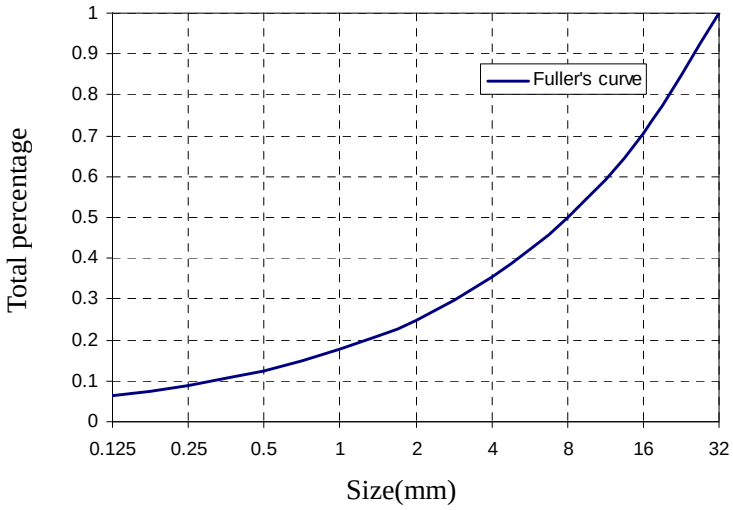

Figure 2. Fuller's grading curve

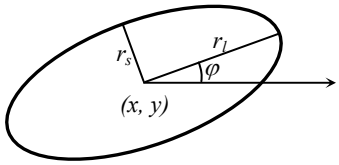

Figure 3. Typical oval particle

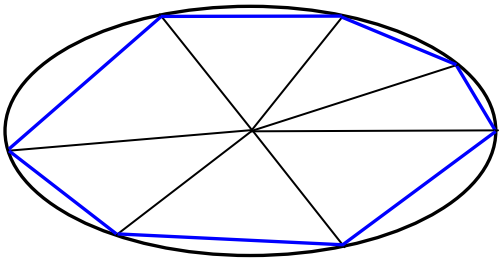

Figure 4. Typical polygonal particle

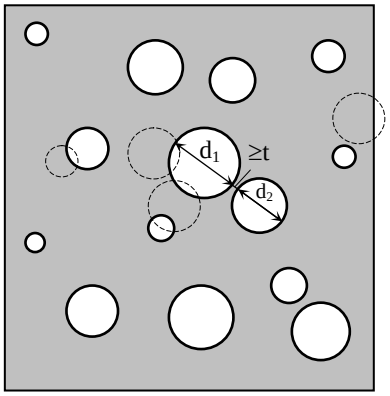

Figure 5. Aggregate placing process

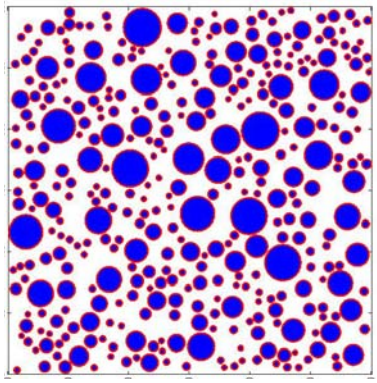

Circular aggregate model

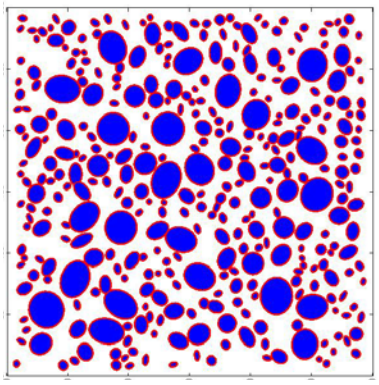

Oval aggregate model

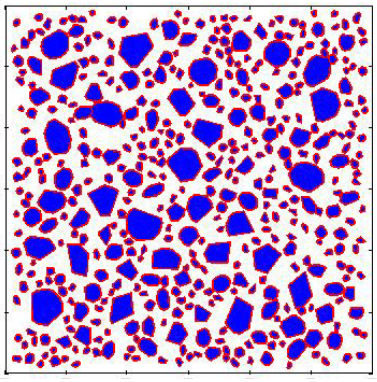

Polygonal aggregate model

Figure 6. Typical aggregate particles

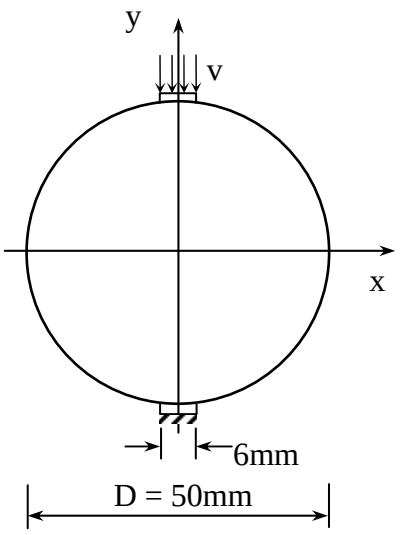

Figure 7. Model geometry and boundary condition for the cylinder specimen

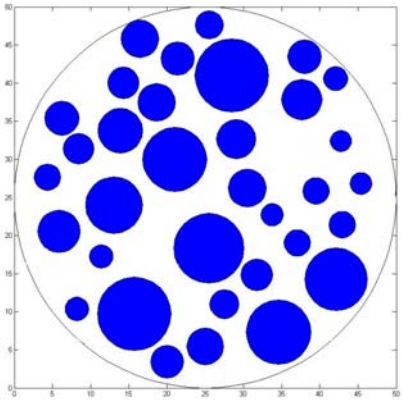

a. random circular aggregate

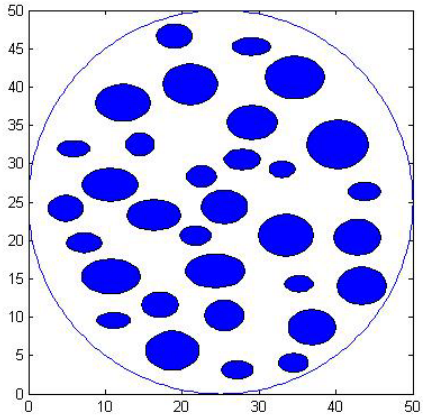

b. random oval aggregate

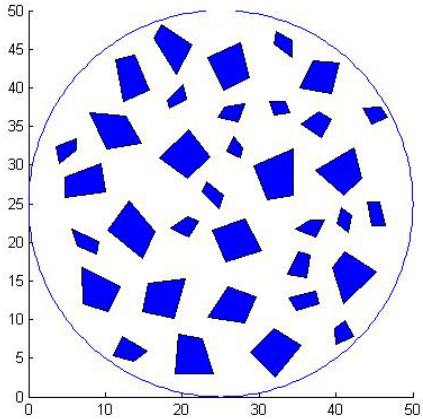

c. random quadrangular aggregate

Figure 8. Coarse aggregate distribution for the cylinder specimen

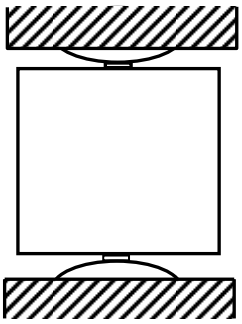

Figure 9. Split tension test setup for the cube specimen

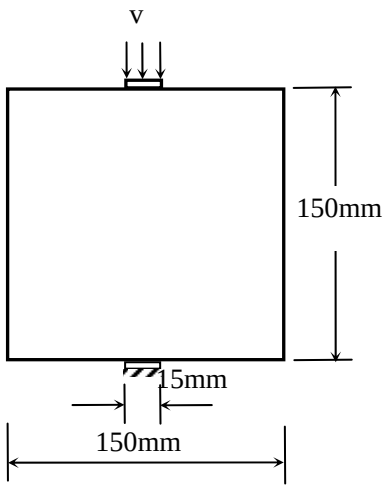

Figure 10. Model geometry for the cube specimen

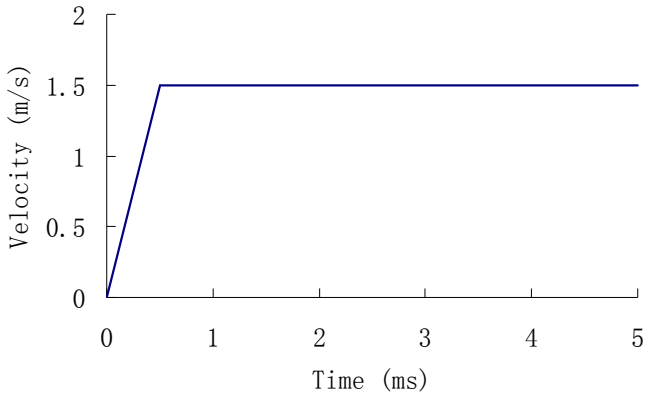

Figure 7. Velocity loading acting on the top boundary

Figure 11. Velocity loading acting on the top boundary of the cube specimen

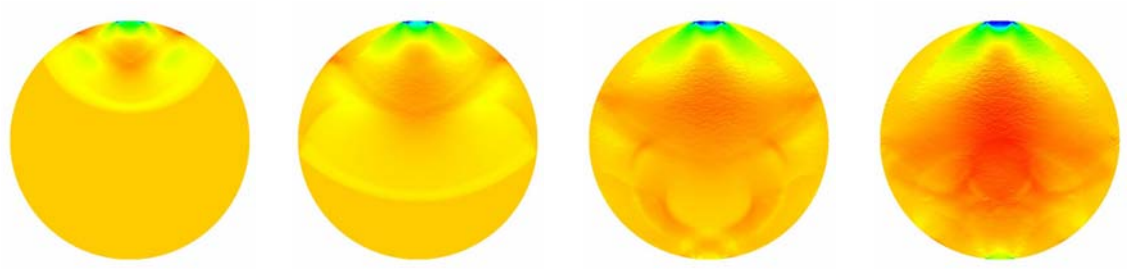

t=0.005 ms t=0.010 ms t=0.015 ms t=0.020 ms

(a) homogeneous model

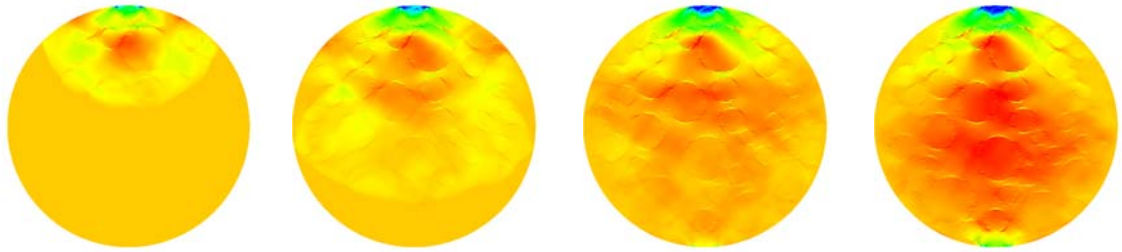

t=0.005 ms t=0.010 ms t=0.015 ms t=0.020 ms

(b) random circular aggregate

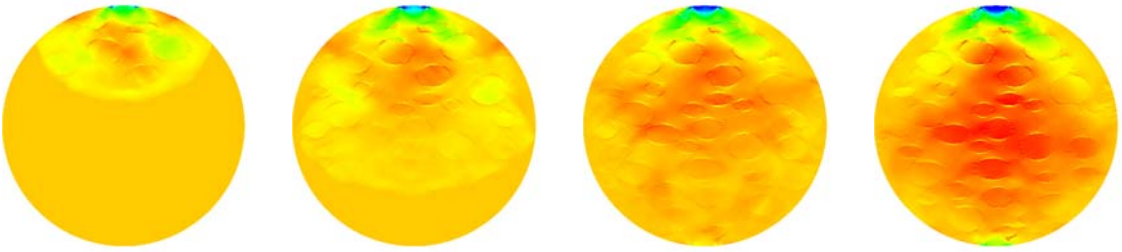

t=0.005 ms t=0.010 ms t=0.015 ms t=0.020 ms

(c) random oval aggregate

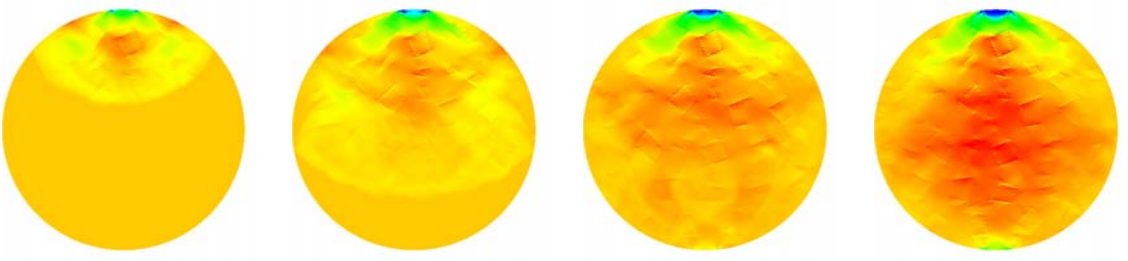

t=0.005 ms t=0.010 ms t=0.015 ms t=0.020 ms

(d) random quadrangular aggregate

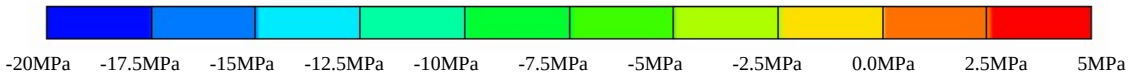

Fig.12 Stress σ_{xx} distribution for different model cases

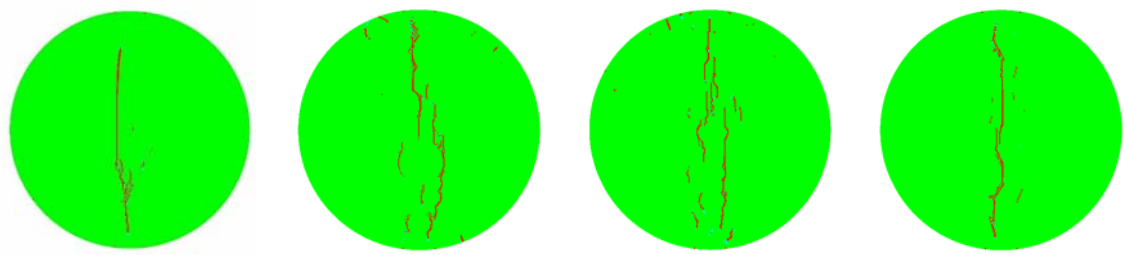

(a) (b) (c) (d)

Figure.13 Failure mode for different cases

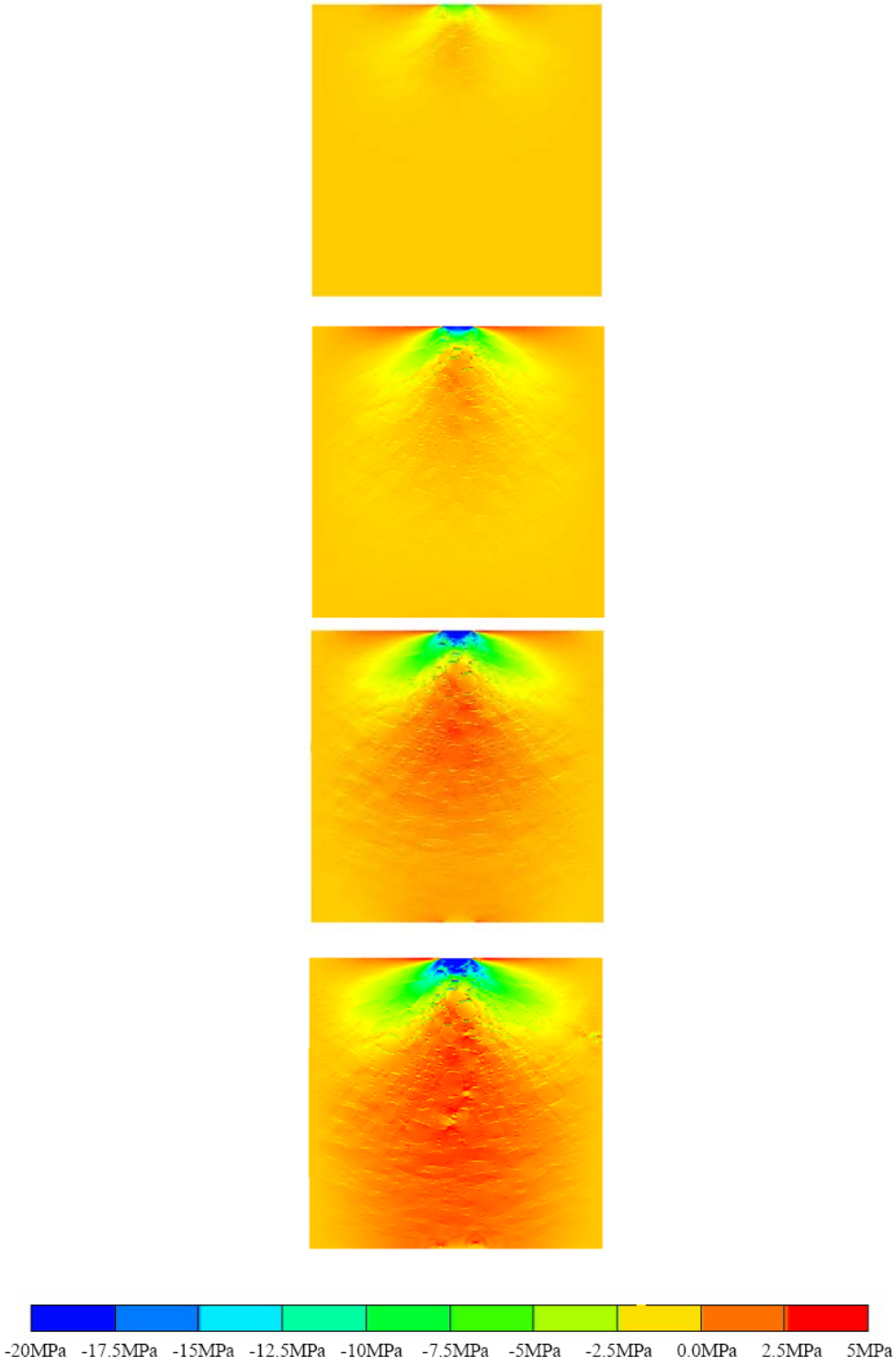

Figure 14. σ_{xx} *distribution at different time instants*

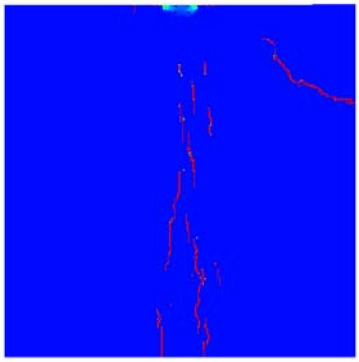

Figure 15. Crack distribution after damage

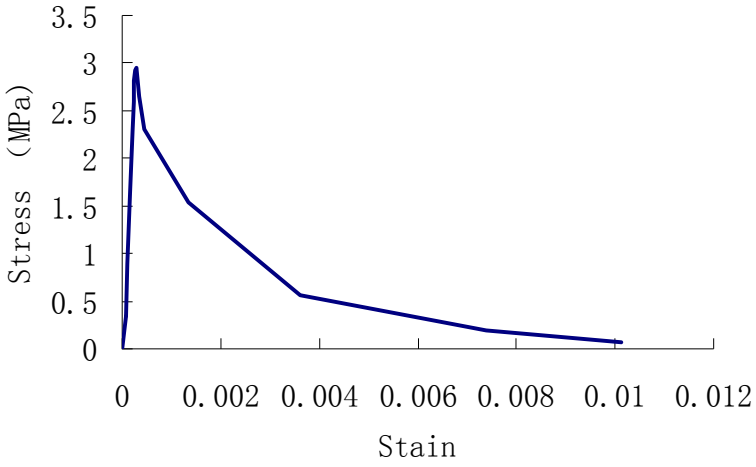

Figure 16. Calculated stress-strain relationship

Table 1 Material parameters

(a) material parameters for mortar matrix and ITZ

	Mortar matrix	ITZ
Solid density ρ_s (kg/m^3)	2.750×10^3	2.750×10^3
Initial density ρ_0 (kg/m^3)	2.1×10^3	1.8×10^3
Initial soundspeed C_0 (m/s)	2.970×10^3	2.572×10^3
Initial compaction pressure p_e (MPa)	32.3	24.3
Solid compaction pressure p_s(MPa)	6000	6000
Shear modulus (GPa)	8.3Gpa	6.24Gpa
Damage parameters α_t, α_c	0.5	0.5
Tensile damage threshold ε_{st0}	2.0×10^{-4}	2.0×10^{-4}
Compressive damage threshold ε_{sc0}	2.0×10^{-3}	2.0×10^{-3}
Tensile strength f_t (MPa)	3.6Mpa	2.7Mpa
Compressive strength f_c (MPa)	45Mpa	33MPa
Cut-off tensile strength f_{ttt} (MPa)	1.8MPa	1.35MPa

(b) material parameters for aggregate

Density ρ_0 (kg/m^3)	2.750×10^3
Bulk modulus K (GPa)	35.7
Shear modulus G (GPa)	17.4
Damage parameters α_t, α_c	0.5
Tensile damage threshold ε_{st0}	3.6×10^{-4}
Compressive damage threshold ε_{sc0}	3.6×10^{-3}
Tensile strength f_t (MPa)	15
Compressive strength f_c (MPa)	200
Cut-off tensile strength f_{ttt} (MPa)	7.5